RSC Advances

PAPER

A theoretical study based on DFT calculations on the different influence of functional groups on the C−H activation process via Pd-catalysed β-X elimination†

Xin Xiang, Zeng-Xia Zhao 🅾* and Hong-Xing Zhang*

We have performed a series of theoretical calculations for palladium-catalyzed β-X elimination reactions. The DFT calculation combined with energy decomposition analysis shows the determining factors of reactivity. Such as, the elemental composition, the structure of different functional groups and the stronger steric repulsions contribution.

Introduction

The transition metal catalyzed C–H activation has been very popular in recent years and has attracted a lot of attention from theoretical chemists.[1–9] Since the 1970s, the coupling organic reactions with Ni, Ru, Rh,[10,11] and Pd[4,12–19] as catalysts have been developed rapidly and attracted the attention of many chemists. Pd, as an important part of catalysts, has attracted the attention of many chemists in recent years, such as, the Kumada, Heck, Suzuki and Negishi[7] groups. Moreover, the ability to functionalize at C–H bonds in the absence of activation groups has great potential in many synthetic pathways. Among them the strategy of using a transition metal to insert starting materials and substitute the functional group at the target position became the most attractive pathway in synthesizing plenty of substrates used in industrial manufacture, the pharmaceutical field and bioengineering departments. In recent years, Engle's group[1,8,14,20–25] has an impressive achievement on the activation of abundant C–O, C–N and C–C bonds via an oxidative addition pathway to form a specific electronically species. To further elucidate the β-X elimination mechanism an experiment was carried out by Engle and co-workers shown in Fig. 1. From these results, we worked out these questions: (i) what is the mechanism of this reaction? (ii) Why is the difference between position of hydroxy made such an influence in **2A-OH** and **HO-2A** of this work? (iii) Why the yield of **N-2A** the lowest in these substituents? In this work, we theoretically investigated sp³ C–H functionalize of various substrates such as four different nucleophile groups shown in Fig. 2, catalyzed by Pd(II) complex to elucidate characteristic features of this reaction and provide

a unique perspective of sp³ C–H functionalization. We selected these substrates to compare reactivity between different functional groups' sp³ C–H bonds, and difference between the presence and the absence of electron with drawing N atom; we made a clear answer to the above-mentioned questions, because this reaction is one of the most important reactions in forming newly redox-neutral approach. C–H provides us a crucial way for making C–C bonds, allowing access to unconventional and structures with high selectivity and efficiency.

Computational details

All geometry optimizations without symmetry restriction were performed by the B3LYP/BSI level (BSI designates the basis set combination of LandL2DZ for Pd atom and 6-31G(d) for other nonmetallic atoms) with Grimme's GD3BJ dispersion corrections.[26–29] Frequency calculation at the same level were performed to ensure the local minima (no imaginary frequencies) or the transition states (only one imaginary frequency), and to derive the thermochemical corrections for the enthalpies and free energies. The intrinsic reaction coordinate (IRC)[30,31] calculations has been employed to track minimum energy paths
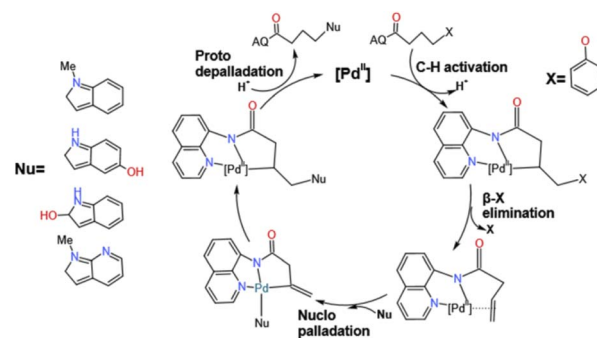
Laboratory of Theoretical and Computational Chemistry, Institute of Theoretical Chemistry, College of Chemistry, Jilin University 130023 Changchun, PR China. E-mail: zhaozx@jlu.edu.cn

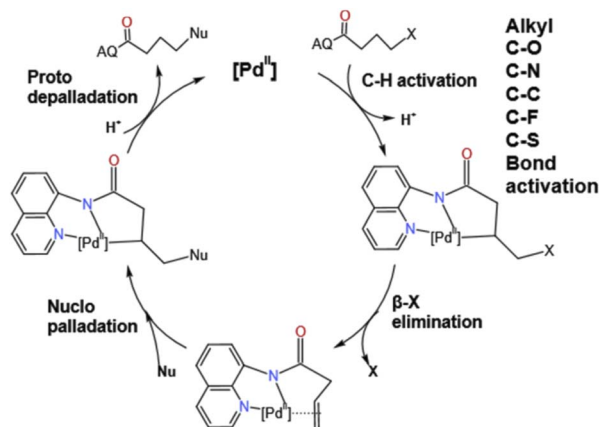Fig. 1 The mechanism of palladium-catalysed reaction of this work.

Fig. 2 The proposed mechanism of the experimental given by the Engle's group.

from transition structure to the corresponding local minima. To evaluate better potential energy, single-point calculations were performed using the M06/BSII level,[32–34] using the acetonitrile as the solvent and SMD as the solvation model, where BSII designates the basis set combination SDD for Pd atom and 6-311++G(d,p) for other atoms. Solvation effect (THF) was evaluated with SMD in this work. In all of the figures that contain energy diagrams, calculated relative Gibbs free energies (kcal mol^{-1}) are presented. All these calculations were carried out using Gaussian16 program.[35] Multiwfn[36] and VMD[37] was used to perform electron distribution. The optimized structures of the species under study were illustrated using CYLview.[38]

Results and discussion

We will describe the detailed catalytic reaction process, active species, rate-determination step here. In addition, we will firstly make a comparison of the effect caused by different nucleophilic groups on the whole reaction process. We will make a comparison of reactivity among various reactive substituents and discuss determining factors of reactivity. In the end, the theoretical prediction of an advantaged suggestion will be presented to provide for laboratory reference, while the oxidative addition of C–H bonds is often an essential substrate activation step in important catalytic hydrocarbon functionalization.

Overview of catalytic

The details of catalytic reaction mechanism and crucial steps were elucidated here. The overall free energy profiles for the catalytic C–H activation process by palladium catalyst was shown in Fig. 3. This reaction occurs through Pd catalyzed cycle; the first step is Pd-catalyst through C–H activation process added to the nitrogen on the benzene ring of the starting materials **1a**'s directing group 8-amino-quinoline (AQ); the second step is the rate determining step, it called β-heteroatom/carbon (β-X) elimination in which the leaving groups leave from the **M4**'s geometry to create another stable geometry which contain unsaturated hydrocarbon/alkene; the third step is nucleo-palladation which from species **M6** turns into species **M9**, in which it across a transition state **TS4**; the final step is the depalladation step also called catalyst regeneration process. Among them we will make a detailed analysis for two important elementary steps: carbon (β-X) elimination and nucleopalladation.
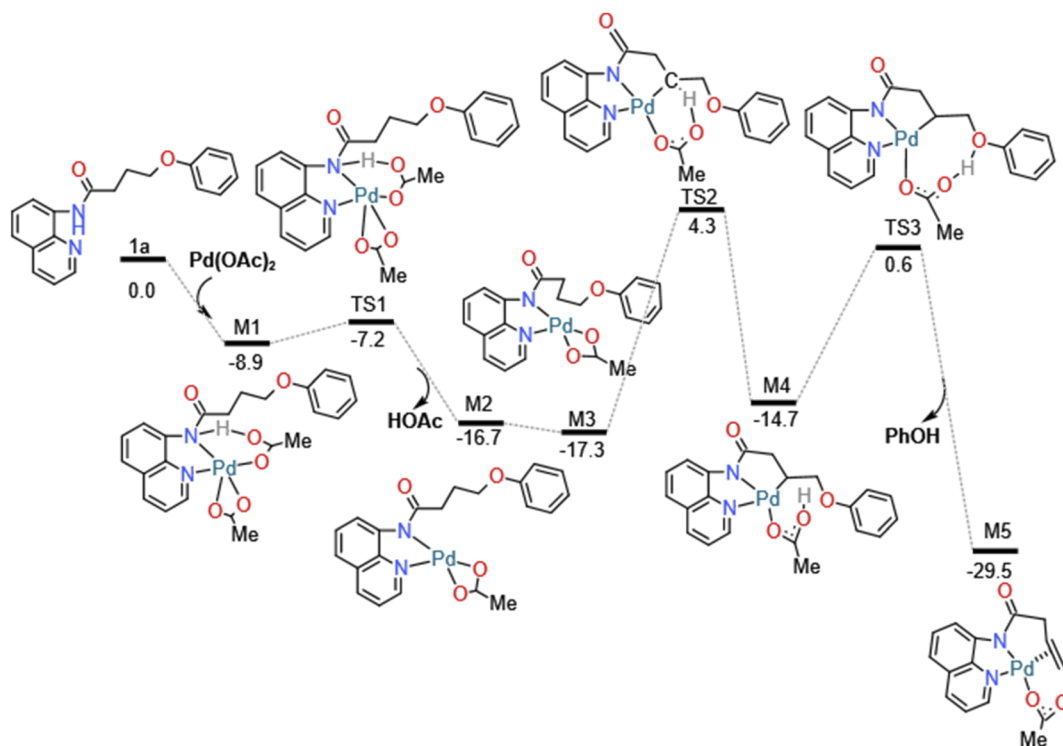

Fig. 3 The first part free energy profile for **HN-2A** catalytic activation.
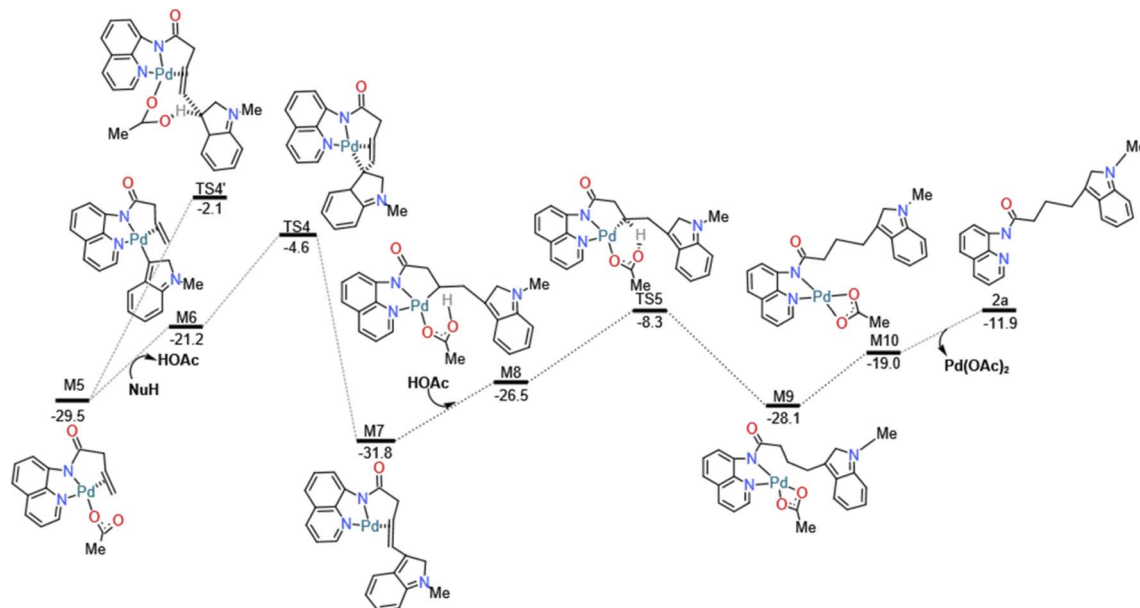
Fig. 4 The second part free energy profile for HN-2A catalytic activation.

As shown in Fig. 3, this reaction initiates from the coordination of the directing group 8-amino-quinoline (AQ) of **1a** to the active Pd(II) center forming the complex **M1** with exoergic by -8.9 kcal mol^{-1}. In order to achieve the relatively remote γ-C's functionalization other than the carbon (α-C) closest to the carbonyl group. By introducing the 8-amino-quinoline (AQ), the directing effect of its bidentate was used to coordinated with pd(II) and activates N–H bond on amide, then followed by the C(sp3)–H activation on carbon chain's γ-C other than α-C to introduce the nucleophilic group to construct C–X bond. In addition, amide bonds are easily hydrolyzed under acidic or alkaline and biological conditions. The N–H activation of the coordinated **1a** could take place *via* the transition state **TS1** to form the five-membered metalacyclic intermediate **M2** and dissociation of acetic acid (HOAc). This N–H bond activation step is a typical concerted metalation/deprotonation mechanism, with a small barrier of 1.7 kcal mol^{-1}, once the N–H bond is activated and an acetic acid is eliminated with the generation of Pd(II) species. In addition, natural bond orbital (NBO) analysis was performed for **TS1** to obtain the atomic charges. The analysis results indicate that the negative charge value of O (-0.711 e) in OAc$^-$ is much lower than that of O atom (-0.575 e) in the carbonyl. The N–H activation process can be illustrated by reduced Pd–N bond distances, 2.04 Å in **M2** (see Fig. S1, ESI†), which means the chemical bond was formed.

In the following β-heteroatom/carbon (β-X) elimination, **M2** isomerize into a more stable intermediate **M3** with exoergic by -0.6 kcal mol^{-1}. After generating the metal complex **M3**, the β-H^2 transfer process to the O^1 atom of acetic acid can be achieved by a barrier of 21.6 kcal mol^{-1}, accompanied by the formation of Pd–C^1 bond. The H transfer process can be illustrated by the gradually elongated C^1–H^2 bond and reduced Pd–C^1 and O^1–H^2 bond, from the 1.10, 4.29 and 4.38 Å in **M3**, 1.42, 2.28 and 1.34 Å in **TS2**, and 2.74, 2.06 and 1.00 Å in **M4** in which acetic acid act as a proton

shuttle. The following H^1 atom can easily attack the O^2 atom of the leaving group and reductive elimination from **M4** can be facilely accomplished *via* the regioselectivity-determining transition state **TS3** generating the more stable π-alkene complex **M5** with exergonic by 14.8 kcal mol^{-1}. In the geometry of **M5**, the C=C bond is almost perpendicular to the Pd heterocyclic plane, so the formed five-membered ring and six-membered ring do not have obvious twisted heterocyclic. The barrier for this process is predicted to be 15.2 kcal mol^{-1}, which is accessible for experimental realization under mild conditions.

And then we considered the syn-nucleopalladation and anti-nucleopalladation pathways according to the energy profile. In the nucleo-palladation step, the nitrogen nucleophile (NuH) attacks the Pd(II) centre forming the intermediate **M6** (in Fig. 4) through ligand exchange. In the meantime, intramolecular syn-nucleopalladation occurs *via* **TS4** (in Table 1) syn-nucleopalladated intermediate **M7**, which is a [5–5–5] thick ring structure, the C=C bond is almost perpendicular to the Pd heterocyclic plane, due to the nucleophilic group takes a position to the unsaturated C atom of olefin, the barrier for this inner-sphere syn-addition pathway is predicted to be 16.6 kcal mol^{-1}, but if measured from the most stable intermediate **M5**, the barrier should be increased to 24.9 kcal mol^{-1}. On the other hand, we also located the anti-addition pathway (**TS4'**) from the complex **M5** is disfavored and requires a barrier of 27.4 kcal mol^{-1}. The formation of the syn-nucleopalladated intermediate **M7** is exoergic by 31.8 kcal mol^{-1}, which can provide thermodynamic driving force to move the reaction forward. The syn-nucleopalladation process can be explanation by the reduced Pd–C^3 bond (2.11 Å), while Natural Bond Orbital (NBO) clearly showed that Pd (0.175 au) attack C (-0.156 au) to form Pd–C^3 bond (2.11 Å), shown in Fig. 5.

After that, in the deprotonation process, the involvement of the acetic acid solvent to coordinate with the Pd center of the
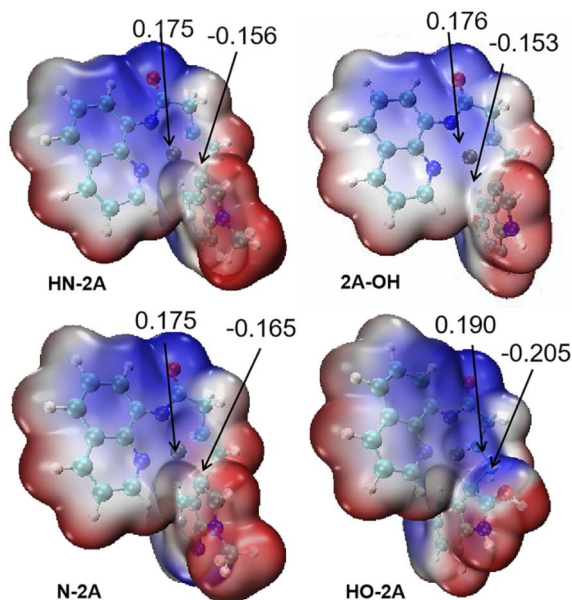
Fig. 5 Natural bond orbital (NBO) analysis and electron-static potential map (ESP) for geometry TS4 of different nucleophile groups.

M7 gives the Pd(II) complex M8. Subsequently, the M8 undergo H-transfer process *via* the transition state TS5 generating the complex M9. The barrier for this H-transfer step is predicted to be 17.2 kcal mol^{-1}. The distorted complex M9 can be readily transformed to the more stable complex M10.

Finally, in the depalladation step, Pd(II) center exchange with acetic acid molecule in the solution, then Pd–N bond eventually dissociates from the N atom of the directing group 8-amino-quinoline (AQ) to release the target nucleophilic substitution 2a, and the palladium-(II) catalyst is regenerated, this catalyst regenerates process is exergonic by 7.1 kcal mol^{-1}.

The influence of affinity groups on the reaction process

In this work, several different nucleophile groups were chosen to compare the different influence on nucleo-palladation HN-2A, 2A-OH, HO-2A and N-2A′, respectively. Among these molecules, HN-2A has a pleased yield, it means that this reaction substrate has a higher conversion rate. For this reason, we choose HN-2A as the criterion, of which different nucleophile groups shows different performance, and to figured out the reason why they show such different manner in this mechanism. In contrast to the structure of N-2A and HN-2A, the difference is that the six-membered ring is benzene in HN-2A while the six-membered ring is pyridine in the N-2A. For the HO-2A and 2A-OH, they not only change the methyl group which on nucleophile's pentagon group into H atom which electron-donating ability is lower than before, but also bring in hydroxyl group into the benzene ring in the same time. The difference between those two species is just the positions of the hydroxyl group in their leaving group. As shown in Fig. 6, the three structures all tend to reduce the electron-donating capacity of nucleophile groups, and the difference in the degree of reduction process needs to be further explained.
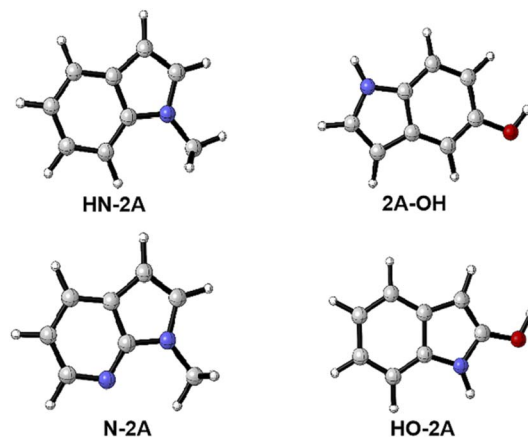

Fig. 6 Several different nuclephile groups choosed in this work.

First of all, the TS4 energy barriers of HN-2A, 2A-OH, N-2A and HO-2A are -4.6 kcal mol^{-1}, 2.7 kcal mol^{-1}, 2.6 kcal mol^{-1}, and 2.6 kcal mol^{-1}, respectively, when cross through the nucleophilic addition step, the transition state TS4 in which the reaction rate of this are 1.6×10^{-6} cm^3 molecula^{-1} s^{-1}, 8.6×10^{-8} cm^3 molecula^{-1} s^{-1}, 9.0×10^{-8} cm^3 molecula^{-1} s^{-1}, and 9.0×10^{-8} cm^3 molecula^{-1} s^{-1}, respectively, shown in Table 2. All of which go through the same process before they turn into the M6 structure. So, we just comparing the rate constant after the bonding of the nucleophile groups. The rate constant of the reactants through TS4 is roughly scaled down. It can be seen that although 2A-OH is slightly slower than HO-2A when it crosses the transition state TS4 in the decisive step, but the rest of other nucleophile groups' reaction rate is basically the same as the reaction yield. We also found that the transition state TS4 of which N-2A has the highest energy barrier and the lowest rate constant. Because the carbon atoms on the benzene ring of N-

Table 1 Kisthelp was used to calculate the reaction rate of the reaction step. Calculated reaction rate constants k for the unimolecular in s^{-1} and bimolecular in cm^3 molecula^{-1} s^{-1}

Species	Molecular	k
TS1	Unimolecular	1.1×10^{14}
TS2	Unimolecular	1.1×10^{12}
TS3	Unimolecular	4.9×10^{12}
TS4	Bimolecular	1.6×10^{-6}
TS5	Unimolecular	1.8×10^{14}

Table 2 The rate constant of the M6 reactants combine with different nucleophile groups to form target products

Species	Yield	Energy barrier (kcal mol^{-1})	k_{TS4} (s^{-1})
HN-2A	90%	-4.6	1.6×10^{-6}
2A-OH	77%	2.7	8.6×10^{-8}
N-2A	19%	2.6	9.0×10^{-8}
HO-2A	6%	2.6	9.0×10^{-8}

2A's nucleophile group is replaced by the N atom who has a stronger electronegativity. In the process of performing transition state **TS4**, due to the stronger N atom electronic absorption ability, the catalyst does not perform as well as **HN-2A** to remove nucleophilic group's H atoms, substrates need to cross a much larger barrier of reaction energy, it also makes a lower reaction rate and a lower production rate. Hence, we can conclude that the lone pair electrons strengthen the benzene ring conjugation, which is mainly caused by the weak electron-withdrawing p(N–C)-π conjugation due to the non-planar p orbital on the nitrogen atom at 3-positions of the pyridine-ring have unshared lone pairs, which form a p-π conjugated system with the π electrons of the benzene ring. It is also noted that the electron cloud density of benzene ring is shifted due to a stronger electronegativity of nitrogen atom, resulting in a more unevenly distributed on the conjugated surface and they can increase the electron cloud density of N on the pyridine ring.

The electron cloud density of pyridine group affects its electron-donating activity, which enhances the difficulty of leaving group to form the substrate **M6**. In addition, **2A-OH** and **HO-2A**'s geometry are similar to each another, they both turn the methyl groups into H atom, meanwhile added a hydroxyl functional group on the nucleophile group, and what worth mentioning is that the difference between them just the position of the hydroxyl group, but there is a big difference in yield, which worth further explanation. First of all, hydroxyl plays different role in **2A-OH** and **HO-2A**, in the state of **2A-OH**, the lone pair on O atom plays more as electron-donor than as nucleophile, but in **HO-2A** situation, the hydroxyl plays as more on nucleophilic groups that have higher electron trapping capacity. Secondly, hydroxyl's electronegativity is larger than methyl, which weaker the nucleophile's H atom leaving capacity, it means the reaction through **2A-OH** and **HO-2A** to forming transition geometry **TS4** need more reaction to receive the same result as **HN-2A** does.

In this work, the deformation energy ($E_{\text{Def-a}}/E_{\text{Def-b}}$) of frag-a and frag-b are defined as follows: $E_{\text{Def-a}} = E_t(\text{frag-a})_{\text{TS}} - E_t(\text{frag-a})_{\text{opt}}$ and $E_{\text{Def-b}} = E_t(\text{frag-b})_{\text{TS}} - E_t(\text{frag-b})_{\text{opt}}$, where subscripts "TS" and "opt" denote the geometry in the TS and the optimized stable geometry, respectively. Which is means the energy difference between the frag-a/b moiety in **TS4** and that in the equilibrium structure of catalyst. The sum of deformation energies indicates the degree of molecule easy or not to across energy barrier. The result shows that **HN-2A**, **N-2A**, **HO-2A**'s deformation energy increase gradually, while $E_{\text{def-sum}}$ is 15.0 kcal mol^{-1}, 15.2 kcal mol^{-1}, 18.5 kcal mol^{-1}, respectively, shown in Table 3. Which indicate that the difficulty of crossing energy barrier is getting harder and harder with the changes in structure, and the results were consistent very well with the yield data.

The energy decomposition analysis (EDA) results are summarized as pie charts shown in Fig. 7 to declare the quantitative contributions of each part of nucleophile–substrate interactions to the overall mechanism in palladation reaction. Each pie chart contains two different effects, steric repulsions and orbital interactions. The weak interactions have been visualized by NICPlots to elucidate the steric effects (see Fig. S8, ESI†). This EDA analysis provides a unique way to identify the dominant factor on how the nucleophile interact on reaction yield. Therefore, a more embedded theoretical investigation on the dominant effect can be performed here to illustrate different effects caused by each nucleophile-substrate. This simple energy decomposition was also performed here. The total energy variation of forming a complex can be decomposed as:

$$\Delta E_{\text{tot}} = E^{\text{complex}} - \sum_i E_i^{\text{frag}}$$
$$= (\Delta E_{\text{els}} + \Delta E_{\text{XC}} + \Delta E_{\text{Pauli}}) + \Delta E_{\text{orb}}$$
$$= \Delta E_{\text{steric}} + \Delta E_{\text{orb}}$$

where ΔE_{els} is electrostatic interaction term, normally negative if the fragments are neutral; ΔE_{els} is change of exchange-correlation energy during complexation process; ΔE_{Pauli} comes from the Pauli repulsion effect between electrons in occupied orbitals of the fragments and is invariably positive, sometimes it is also referred to as exchange-repulsion term. For convenience, it is customary to combine these three terms as steric term (ΔE_{steric}).

ΔE_{orb} in above formula is orbital interaction term, it arises from the mix of occupied MOs and virtual MOs, and it exhibits polarization and charge-transfer effects. If the combined wavefunction is used as initial guess for complex, then ΔE_{orb} can be evaluated by subtracting the first SCF iteration energy from the last SCF iteration energy:

$$\Delta E_{\text{orb}} = E_{\text{SCF,last}} - E_{\text{SCF,1st}}$$

Note that $E_{\text{SCF,last}} = E_{\text{complex}}$. Obviously, we have below relationship.

$$\Delta E_{\text{steric}} = \Delta E_{\text{tot}} - \Delta E_{\text{orb}} = E_{\text{SCF,1st}} - \sum_i E_i^{\text{frag}}$$
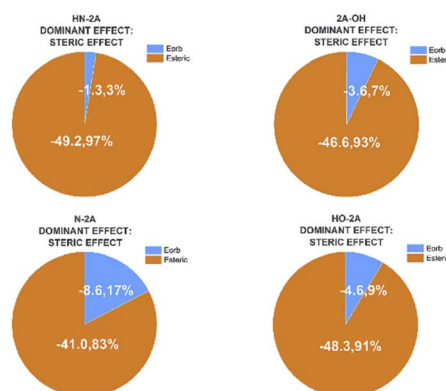
Fig. 7 Energy contributions of different types interactions of nucleophile substrate in Pd(OAc)$_2$ catalyzed system.

Table 3 Deformation energy (E_{def}) of fragments a and b

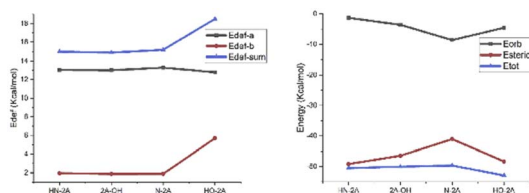| Species	$E_{\text{def-a}}$ (kcal mol^{-1})	$E_{\text{def-b}}$ (kcal mol^{-1})	$E_{\text{def-sum}}$ (kcal mol^{-1})
HN-2A	13.0	1.9	14.9
2A-OH	13.0	1.9	14.9
N-2A	13.3	1.9	15.2
HO-2A	12.8	5.7	18.5

Fig. 8 The results of deformation energy analysis and EDA studies performed in this mechanism.

While absolute and also relative orbital contributions are lager in the **HN-2A** complex, with a weaker steric interaction result in the slightly weaker bond strength. The bonding picture of these four species are very different from each other. Without the attractive contributions of -41.0 kcal mol^{-1} arising from steric interactions, **N-2A** would not be stable. And the bond dissociation energy of **N-2A** is slightly larger than the rest of other substrates. The decomposition of the **HN-2A, 2A-OH, N-2A, HO-2A**'s total interaction shows that -49.2 kcal mol^{-1}, -46.5 kcal mol^{-1}, -41.0 kcal mol^{-1} and -48.3 kcal mol^{-1} comes from steric effect and -1.3 kcal mol^{-1}, -3.6 kcal mol^{-1}, -8.6 kcal mol^{-1} and -4.6 kcal mol^{-1} comes from orbital contribution, respectively, shown in Fig. 8. The EDA shows that the dominant increase come from stronger steric contribution.

Conclusions

DFT calculation was carried out to simulate the origin of difference manner carried out by nucleophile group, and we get a deeper perspective conversion about these different groups. Firstly, we get the mechanism about the outset of the works, which contain four vital step, N–H activation, β-X elimination, nucleophilic addition and catalyst regeneration. Secondly, we find out the relationship between the structure and reactivity, and how did these differences perform by chemical bond, energy barrier, NBO, BDE. Through the analysis of the chemical bond between the target γ-C and Nu group, we can see that the better the electron donating ability of the Nu group's five-membered ring, has the lower the reaction energy barrier needs to be crossed when combining γ-C atom, and the smaller steric interactions between the target γ-C and Nu groups, and the greater the orbital interactions of the formed chemical bond showed by the EDA analysis. Meanwhile, BDE analysis showed that compared with **HO-2A**'s group with the lowest yield, the bond dissociation energy of other Nu groups was relatively high, indicating that the more stable target chemical bond. Natural Charge Population obtained by NBO analysis showed the same electron flow trend from γ-C to Nu group. Finally, the rate-determining step is the nucleophilic addition step, while to cross **TS4** energy barrier, and the EDA shows the steric repulsions contribute to the majority of the intra-molecular interactions.

Conflicts of interest

There are no conflicts to declare.

Notes and references

1 K. S. Yang, J. A. Gurak, Jr., Z. Liu and K. M. Engle, *J. Am. Chem. Soc.*, 2016, **138**, 14705–14712.

2 A. Simaioforidou, M. Papastergiou, A. Margellou, D. Petrakis and M. Louloudi, *J. Mol. Catal. A: Chem.*, 2017, **426**, 516–525.

3 M. Moselage, J. Li and L. Ackermann, *ACS Catal.*, 2015, **6**, 498–525.

4 M. Maffei, G. Giacoia, R. Mancuso, B. Gabriele, E. Motti, M. Costa and N. Della Ca', *J. Mol. Catal. A: Chem.*, 2017, **426**, 435–443.

5 H. S. Haniff, L. Knerr, X. Liu, G. Crynen, J. Bostrom, D. Abegg, A. Adibekian, E. Lekah, K. W. Wang, M. D. Cameron, I. Yildirim, M. Lemurell and M. D. Disney, *Nat. Chem.*, 2020, **12**, 952–961.

6 Y. Han and H. V. Huynh, *Dalton Trans.*, 2011, **40**, 2141–2147.

7 X. Fu, Q. Qi, S. Xu and E.-i. Negishi, *Org. Lett.*, 2021, **23**, 8984–8988.

8 X. Chen, K. M. Engle, D. H. Wang and J. Q. Yu, *Angew. Chem.*, 2009, **48**, 5094–5115.

9 A. N. Bilyachenko, M. S. Dronova, A. I. Yalymov, F. Lamaty, X. Bantreil, J. Martinez, C. Bizet, L. S. Shul'pina, A. A. Korlyukov, D. E. Arkhipov, M. M. Levitsky, E. S. Shubina, A. M. Kirillov and G. B. Shul'pin, *Chemistry*, 2015, **21**, 8758–8770.

10 Y. Wu, H. Yu, Y. Guo, X. Jiang, Y. Qi, B. Sun, H. Li, J. Zheng and X. Li, *Chem. Sci.*, 2019, **10**, 10459–10465.

11 S. Ruiz, F. J. Sayago, C. Cativiela and E. P. Urriolabeitia, *J. Mol. Catal. A: Chem.*, 2017, **426**, 407–418.

12 A. L. Wierschen, N. Romano, S. J. Lee and M. R. Gagne, *J. Am. Chem. Soc.*, 2019, **141**, 16024–16032.

13 E. Silarska, M. Majchrzak, B. Marciniec and A. M. Trzeciak, *J. Mol. Catal. A: Chem.*, 2017, **426**, 458–464.

14 M. L. O'Duill and K. M. Engle, *Synthesis*, 2018, **50**, 4699–4714.

15 S. K. Nimmagadda, M. Liu, M. K. Karunananda, D. W. Gao, O. Apolinar, J. S. Chen, P. Liu and K. M. Engle, *Angew. Chem.*, 2019, **58**, 3923–3927.

16 Y. Makida, H. Ohmiya and M. Sawamura, *Chem. - Asian J.*, 2011, **6**, 410–414.

17 C. Lin, F. Gao and L. Shen, *Adv. Synth. Catal.*, 2019, **361**, 3915–3924.

18 T. He, J. C. Buttner, E. F. Reynolds, J. Pham, J. C. Malek, J. M. Keith and A. R. Chianese, *J. Am. Chem. Soc.*, 2019, **141**, 17404–17413.

19 H. Azizollahi, V. P. Mehta and J. A. Garcia-Lopez, *Chem. Commun.*, 2019, **55**, 10281–10284.

20 J. Derosa, V. T. Tran, M. N. Boulous, J. S. Chen and K. M. Engle, *J. Am. Chem. Soc.*, 2017, **139**, 10657–10660.

21 D. W. Gao, Y. Gao, H. Shao, T. Z. Qiao, X. Wang, B. B. Sanchez, J. S. Chen, P. Liu and K. M. Engle, *Nat. Catal.*, 2020, **3**, 23–29.

22 J. A. Gurak, V. T. Tran, M. M. Sroda and K. M. Engle, *Tetrahedron*, 2017, **73**, 3636–3642.

23 J. A. Gurak, Jr., K. S. Yang, Z. Liu and K. M. Engle, *J. Am. Chem. Soc.*, 2016, **138**, 5805–5808.

24 L. J. Oxtoby, Z. Q. Li, V. T. Tran, T. G. Erbay, R. Deng, P. Liu and K. M. Engle, *Angew. Chem.*, 2020, **59**, 8885–8890.

25 V. T. Tran, J. A. Gurak, Jr., K. S. Yang and K. M. Engle, *Nat. Chem.*, 2018, **10**, 1126–1133.

26 P. Hay and W. Wadt, Potentials for K to Au Including the Outermost Core Orbitals, *J. Chem. Phys.*, 2021, 82.

27 P. C. Hariharan and J. A. Pople, *Theor. Chim. Acta*, 1973, **28**, 213–222.

28 A. Becke, *Phys. Rev. A*, 1988, **38**, 3098–3100.

29 C. Lee, W. Yang and R. G. Parr, *Phys. Rev. B*, 1988, **37**, 785–789.

30 K. Fukui, *J. Phys. Chem.*, 1997, **74**, 4161–4163.

31 K. L. Schuchardt, B. T. Didier, T. Elsethagen, L. Sun, V. Gurumoorthi, J. Chase, J. Li and T. L. Windus, *J. Chem. Inf. Model.*, 2007, **47**, 1045–1052.

32 E. A. P. t. Denis Jacquemin, I. Ciofini, C. Adamo, R. Valero, Y. Zhao and D. G. Truhlar, *J. Chem. Theory Comput.*, 2010, **6**, 2071–2085.

33 Y. Zhao and F. Chen, *J. Multivariate. Anal.*, 2008, **99**, 215–231.

34 Y. Z. a. D. G. Truhla, *J. Phys. Chem. A*, 2006, **110**, 13126–13130.

35 M. J. Frisch, *et al.*, *Gaussian 16, Revision A.03*, Gaussian, Inc., Wallingford CT, 2016.

36 T. Lu and F. Chen, *J. Comput. Chem.*, 2012, **33**, 580–592.

37 W. Humphrey, A. Dalke and K. Schulten, *J. Mol. Graphics*, 1996, **14**(33–38), 27–38.

38 CYLview, 1.0b; Legault, C. Y., Universite de Sherbrooke, 2009, http://www.cylwe.org.